

Phase Diagram of the Superfluid Phases of ^3He in 98% Aerogel

G. Gervais¹, K. Yawata¹, N. Mulders² and W.P. Halperin¹

¹*Department of Physics and Astronomy, Northwestern University, Evanston, Illinois, 60208 USA*

²*Department of Physics and Astronomy, University of Delaware, Newark, Delaware, 19716 USA*

(October 25, 2019)

The phase diagram of the superfluid phases of ^3He in 98% aerogel was determined in the range of pressure from 15 to 33 bars and for fields up to 3 kG using high-frequency sound. The superfluid transition in aerogel at 33.4 bars is field independent from 0 to 5 kG and shows no evidence of an $A_1 - A_2$ splitting. The first-order transition between the A and B-phases is suppressed by a magnetic field, and exhibits strong supercooling at high pressures. We show that the equilibrium phase in zero applied field is the B-phase with at most a region of A-phase $\lesssim 20 \mu\text{K}$ just below T_c at a pressure of 33.4 bars. This is in contrast to pure ^3He which has a large stable region of A-phase and a polycritical point. The quadratic coefficient for magnetic field suppression of the AB-transition, $g_a(\beta)$, was obtained. The pressure dependence of $g_a(\beta)$ is markedly different from that for the pure superfluid, $g_0(\beta)$, which diverges at a polycritical pressure of 21 bars. We compare our results with calculations from the homogeneous scattering model for $g_a(\beta)$, defined in a Ginzburg-Landau theory in terms of strong-coupling parameters β . We find qualitatively good agreement with the experiment if the strong-coupling corrections are rescaled from known values of the β 's for pure ^3He , reduced by the suppression of the superfluid transition temperature. The calculations indicate that the polycritical pressure in the aerogel system is displaced well above the melting pressure and out of experimental reach. We cannot account for the puzzling supercooling of the aerogel AB-transition in zero applied field within the framework of known nucleation scenarios.

PACS numbers:67.57.Pq,67.57.Bc,64.60.Kw

I. INTRODUCTION

Quenched disorder in condensed matter systems is manifest in a wide variety of materials from glassy solids and liquid crystals to the mixed state of superconductors. It arises in diverse phenomena ranging from cosmological models for the evolution of the universe to vortex tangles in superfluid ^4He . Disorder in superfluid ^3He is of special interest since the order parameter structure of this superfluid is non-trivial, although well known, and its various phases exhibit a number of spontaneously broken symmetries. Quenched disorder in a superfluid can be generated extrinsically by a random impurity field with inhomogeneity on a length scale short compared to the coherence length. In the present case this is achieved by imbibing ^3He into silica aerogel, a highly-porous material made of randomly inter-connected strands of SiO_2 .

Aerogels have been used to study liquid crystals¹, superfluid ^4He ², ^3He - ^4He mixtures³ and superfluid ^3He ^{4,5}. Glassy effects have been observed in the liquid crystal-aerogel systems. In ^3He - ^4He mixtures a profound influence of aerogel on the phase diagram³ was reported. Superfluid ^3He in aerogel was found to have a suppressed, but relatively sharp, transition temperature and the order parameter appears to be reduced^{4,5}. However, the nature of the phase diagram, and identification of the thermodynamically stable phases, have not yet been clearly established. Here we report the use of high resolution transverse acoustic impedance to map out this phase diagram.

The ^3He -A and -B superfluid phases were discovered in 1972 by Osheroff, Richardson and Lee⁶. The or-

der parameter is now established to be a p -wave spin-triplet which has two thermodynamically stable superfluid phases in zero field. The A-phase is the axial state which separately breaks spin and orbit rotational symmetries. The B-phase is the isotropic state which breaks relative spin-orbit symmetry. The stability of the A-phase over the B-phase at elevated pressure, above the polycritical pressure of 21 bars in zero field, is a consequence of strong coupling in the quasiparticle interactions. After 30 years of extensive experimental and theoretical investigation ^3He is the best understood of all unconventional superfluids or superconductors. Motivation to investigate disorder in this superfluid derives in part from our need to understand impurity effects in this, and in similar, unconventionally paired systems. New families of superconducting materials such as Sr_2RuO_4 ⁷, URhGe ⁸, and organic conductors⁹ may be unconventional superconductors, and in some cases, a p -wave structure has been suggested.

At millikelvin temperatures ^3He is the purest material in nature. Its properties have been investigated extensively as a system entirely free of impurity scattering other than at surfaces. The influence of aerogel on ^3He is to suppress the transition retaining a narrow width and to alter the behavior of the superfluid phases. In contrast, for surface scattering, the orientation and the amplitude of the order parameter are both constrained and the superfluid becomes spatially inhomogeneous. The use of highly-porous aerogels to introduce impurity scattering in ^3He has provided a significant opportunity to learn about unconventional pairing states. The first observations of superfluidity were torsional oscillator ex-

periments to measure the superfluid density performed at Cornell⁴ and Nuclear Magnetic Resonance (NMR) at Northwestern^{5,10}. These results were found to be consistent with theoretical models for impurity scattering¹¹. In its simplest form, the Homogeneous Scattering Model (HSM), the suppression of the superfluid transition is given by the well-known Abrikosov-Gorkov formula

$$\ln\left(\frac{T_{c0}}{T_{ca}}\right) = \Psi\left(\frac{1}{2} + \frac{1}{2} \frac{\xi_0}{l_{tr}} \frac{T_{c0}}{T_{ca}}\right) - \Psi\left(\frac{1}{2}\right) \quad (1)$$

where $T_{ca}(T_{c0})$ is the superfluid transition temperature of the aerogel (bulk) system, $\xi_0 \equiv \hbar v_f / 2\pi k_B T_{c0}$ is the bulk coherence length, and l_{tr} is the transport mean free path. These earlier results triggered numerous experimental investigations^{12–17} and theoretical work^{11,18–25} aimed at characterizing and understanding the properties of the ‘dirty’ superfluid formed inside the aerogel matrix. However, the identification of the superfluid state in the ³He-aerogel system has been controversial, and only recently has there been agreement as to which are the superfluid phases observed.

The first NMR measurement in pure ³He and 1.2 kG suggested a superfluid in an equal-spin pairing (ESP) state⁵ similar to the bulk A-phase. With ⁴He additions a non-ESP state was found¹⁰ like the bulk B-phase. NMR measurements at lower fields (\sim 50 G) without ⁴He found evidence for a B-phase superfluid in aerogel¹² and Barker *et al.*¹⁵ found a transition between a ESP and a non-ESP state at 284 G with ⁴He coverage. This transition was found to supercool quite readily and was identified to take place between A and B superfluids, but it should be kept in mind that the orbital symmetry of the order parameter in aerogel has not yet been determined. The aerogel AB-transition was also observed recently by a vibrating viscometer at low pressures²⁶, and was studied near the bulk polycritical pressure (PCP) using high-frequency sound²⁷. The reason for covering the strands with some ⁴He (2 or more atomic layers) is to replace magnetic solid ³He that contributes to measurement of the ³He magnetization and may also affect the nature of the scattering and possibly properties of the dirty superfluid. In the present work, we present a comprehensive acoustics study of the phase diagram of the A and B-superfluid phases of ³He in a 98% aerogel without ⁴He and from 0 to 3 kG.

II. EXPERIMENTAL

High-frequency sound (\sim MHz) has proven to be a powerful tool to study the properties of pure ³He in the normal Fermi liquid and in the superfluid state. For example, Landau’s seminal prediction of collisionless sound, called zero-sound, in a Fermi liquid was experimentally verified with high-frequency sound attenuation measurements²⁸. High-frequency sound also couples strongly to the order parameter collective modes

(OPCM) of the superfluid and numerous OPCM have been observed in both the A and B-phases of pure ³He (see²⁹ for a review). Transverse sound was predicted to exist in normal ³He by Landau, and was shown to propagate in ³He-B from the observation of an acoustic Faraday effect³⁰. In what follows, we describe a technique used to probe the phase diagram of ³He in aerogel using both transverse and longitudinal high-frequency sound waves.

The acoustic technique is similar to that reported previously^{31,32} and a schematic of our acoustic cavity is depicted in Fig.1. The cavity was formed with two quartz transducers separated by two parallel stainless steel wires of diameter $d = 270 \mu\text{m}$ ³³. One transducer was AC-cut for transverse sound, and the other X-cut for longitudinal sound, with a diameter of 9.5 mm. Their fundamental frequencies were 4.8 MHz and 2.9 MHz, respectively. This arrangement allowed us to perform experiments with either transverse or longitudinal sound. The aerogel was grown *in situ*, in the volume between the transducers. Each transducer has two active sides; one probes the aerogel-filled cavity, and the other the bulk liquid outside the cavity. All experiments were performed with pure ³He which was verified to contain less than 250 ppm of ⁴He, much less than the amount required to cover the aerogel strands with one atomic layer of ⁴He.

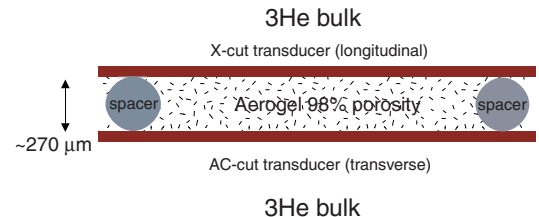


FIG. 1. Schematics of the acoustic cavity. The X-cut (longitudinal sound) and AC-cut (transverse sound) transducers are separated by $270 \mu\text{m}$ spacers and the 98% porous aerogel was grown *in situ*. Each transducer has two active sides; one probes the aerogel-filled cavity while the other probes the bulk liquid outside the cavity.

The electrical impedance of the transducers was measured using a continuous wave spectrometer. The measurements were performed at a fixed frequency corresponding to odd harmonics of the fundamental resonance, with a frequency modulation of 400 Hz and modulation amplitude of 3 kHz. In the case of longitudinal sound, the medium inside the cavity is of sufficiently low attenuation that a standing wave pattern is established throughout the cavity. Small changes in the attenuation and velocity, induced by changes in temperature or pressure, produced changes in the electrical impedance of the transducers that can be detected by the spectrometer^{31,33}. For transverse sound, the highly attenuating medium prohibits the existence of well-defined standing waves and the measurement is similar to that of an acoustic impedance measurement³². It is not possible

with this technique to separate individual contributions from attenuation, sound velocity, or coupling to collectives modes in the transverse acoustic impedance. However, we have found that, at low frequencies ($\lesssim 10$ MHz), the transverse sound impedance changes abruptly at all of the known phase transitions in each of the bulk and aerogel superfluids, Fig.2.

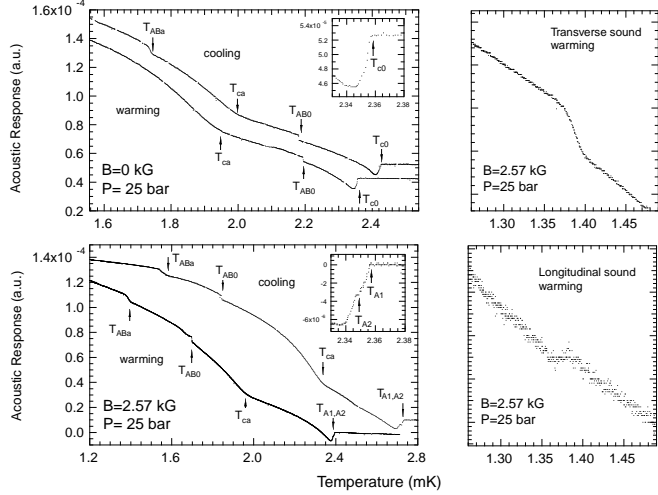


FIG. 2. Left: transverse acoustic response at 25 bars and zero applied field (upper panel) and 2.57 kG (lower panel). In each panel, the data in the upper (lower) trace is taken on cooling (warming). The temperature scale is for warming only; for cooling the traces were offset for clarity. The various transitions in the bulk and aerogel superfluids are indicated by arrows. The inset is an enlarged view of the bulk superfluid transition T_{c0} in zero field (upper), and 2.57 kG (lower) which shows the bulk A_1 and A_2 transitions. Right: an enlarged view of the aerogel AB-transition on warming is shown at 25 bars and 2.57 kG for the acoustic response of transverse sound at 8.691 MHz in the upper panel and longitudinal sound at 14.635 MHz in the lower panel.

The transverse acoustic response at 8.691 MHz and a pressure of 25 bars is shown in the left panels of Fig.2 on cooling (upper trace) and warming (lower trace) and at zero (upper panel) and 2.57 kG applied magnetic field (lower panel). The phase transitions in the bulk liquid and the aerogel are denoted by arrows. On cooling, and in zero applied field, we successively observed the bulk superfluid (T_{c0}), bulk AB (T_{AB0}), aerogel superfluid (T_{ca}) and aerogel AB (T_{ABa}) transitions. The thermometry scales for cooling and warming are different. The scale shown in the figure is for slow warming such that equilibrium is assured between the LCMN thermometer used in low field, the melting curve thermometer, and the aerogel sample. For the results in Fig.2 and Fig.4, we corrected the thermometry for the more rapid cooling experiments using the temperature dependence of the acoustic impedance established in equilibrium during warming. This provides a convenient and intrinsic secondary thermometer, but for clarity the cooling traces are off-

set. When a magnetic field is applied, we also observed the bulk $A_1 - A_2$ splitting as a ‘knee’ in the acoustic response, as shown in the inset of the lower left panel. The bulk A_1 and A_2 -transitions are completely resolved in the acoustic trace at a field of ~ 5 kG and above.

In the right panels of Fig.2 we show a direct comparison of the signatures from transverse and longitudinal sound for the aerogel AB-transition observed on warming at 25 bars and 2.57 kG. A small jump in the acoustic trace of longitudinal sound, coincident in temperature with that of transverse sound, was observed when the AB-transition occurred at temperatures sufficiently well below T_{ca} . The condition for observing the signature in longitudinal sound was that the transition be either supercooled or that it appear on warming in a field $B \gtrsim 2$ kG. However, we cannot determine whether this jump in the longitudinal sound trace arises from a change in attenuation due to collective modes, or from quasiparticle excitations. The observation of the aerogel AB-transition in longitudinal sound ensures that the transition observed with transverse sound is not a local effect occurring near the surface of the transducer. We have shown previously^{31,33} that a well-defined longitudinal sound mode can be established in our acoustic cavity, and therefore the AB-transition observed with this mode reflects the behavior of the superfluid over the entire aerogel sample. We have also verified that the change of slope in the transverse acoustic trace labeled T_{ca} corresponds to the temperature at which the attenuation of longitudinal sound decreases at the onset of the superfluid transition³¹. However, the wider range of observability of the aerogel AB-transition by transverse sound, as compared with longitudinal sound, and its higher precision make it a better tool to map out the phase diagram of ^3He in 98% aerogel. The frequency dependence of the bulk superfluid transition T_{c0} , as observed with transverse sound, was also systematically studied at a pressure of 17 bars and for frequencies ranging from 3 MHz to 55 MHz. We found that the transverse acoustic signature signaling T_{c0} is weakly frequency dependent but that it recovers the transition temperature T_{c0} in the low-frequency limit, $\lesssim 10$ MHz. The transition temperatures observed in our sample are in excellent agreement with those reported elsewhere^{5,15,34} for the same density of aerogel. In what follows, the (P,T,B) phase diagram of ^3He in aerogel was determined using transverse sound at a frequency of 8.691 MHz.

III. RESULTS AND DISCUSSION

A. P-T-B dependence of the AB-transition in aerogel

One of the key issues in the study of superfluid ^3He in aerogel is to determine in what way the superfluid phase diagram is modified by impurity scattering. Unlike s -

wave superconductors for which only magnetic impurity scattering is pair breaking, p -wave Cooper pairs are sensitive to all forms of scattering. For superfluid ^3He in aerogel, there is now general agreement that impurity scattering suppresses the superfluid transition temperature and the amplitude of the order parameter, and that a non-ESP phase similar to the bulk B-phase is favored near zero field. However, most experiments have been performed in different regions of P, T, and B and also under different experimental conditions, *e.g.* with or without ^4He preplating on the aerogel strands and with different aerogel densities. In particular, the phase diagram of the pure superfluid phases of pure ^3He in 98% aerogel has not been established; the zero-field phase diagram is largely unknown. We emphasize that only the spin structure of the pairing state of ^3He in aerogel has been identified through NMR measurement of the magnetization^{10,15} or the stability of the transition in a magnetic field^{26,27}. In the latter case, assuming triplet pairing, we can infer the spin component of the order parameter (ESP or non-ESP) from the field dependence of the phase boundaries. The orbital symmetry is more elusive. For example, it would be helpful to investigate the OPCM which couple to orbital degrees of freedom of the order parameter, but they have not yet been observed³¹. Nonetheless, we use the earlier notation^{15,26,27} ‘A’ and ‘B’ for the aerogel superfluid phases corresponding to ESP and non-ESP states, by analogy with the bulk, and we discuss later implications from our measurements for the orbital symmetry of the aerogel superfluid.

The phase diagrams of the aerogel AB-transition as a function of B^2 and for various pressures are shown in Fig.3. The triangles denote the superfluid transitions, T_{ca} , as determined by the change of slope in the transverse acoustic trace, the filled circles are the equilibrium AB-transitions taken on slow warming, and the empty circles are the supercooled AB-transitions. The long-dashed lines show the average values of T_{ca} and the dotted lines are extrapolations to zero field. With our technique, we were unable to observe directly the aerogel AB-transitions on warming at fields below 1.4 kG, *i.e.* for $T_{ABa}/T_{ca} \gtrsim 0.9$. An independent check on the validity of our extrapolation to zero field will be discussed below.

The magnetic field independent transition from normal to superfluid state, and field-dependent transitions from A to B-superfluids strongly suggest that these are transition between normal fluid to ESP superfluid states, and between ESP and non-ESP states, as in the bulk. The strong supercooling of the AB-transition, even in zero applied field, shows that the transition is first-order. However, there are key differences in the aerogel phase diagram as compared to the bulk. In particular, the zero-field equilibrium region of aerogel A-phase is extremely narrow, $\lesssim 20 \mu\text{K}$ at 33.4 bars, if it exists at all.

In order to locate the AB-phase boundary at 33.4 bars in zero applied field, we have performed a series of temperature sweeps in which the temperature was slowly raised from low-temperature ($\sim 0.6 \text{ mK}$) to a temper-

ature in the vicinity, but slightly less than, T_{ca} , and then rapidly cooled. If the AB-phase boundary were reached on warming, the supercooled AB-transition would be observed on cooling, whereas in the opposite case the aerogel superfluid would remain in the B-phase with no evidence for an AB-transition. This procedure depends on the absence of what is called a memory effect for secondary nucleation which we verified independently in modest magnetic fields³⁵.

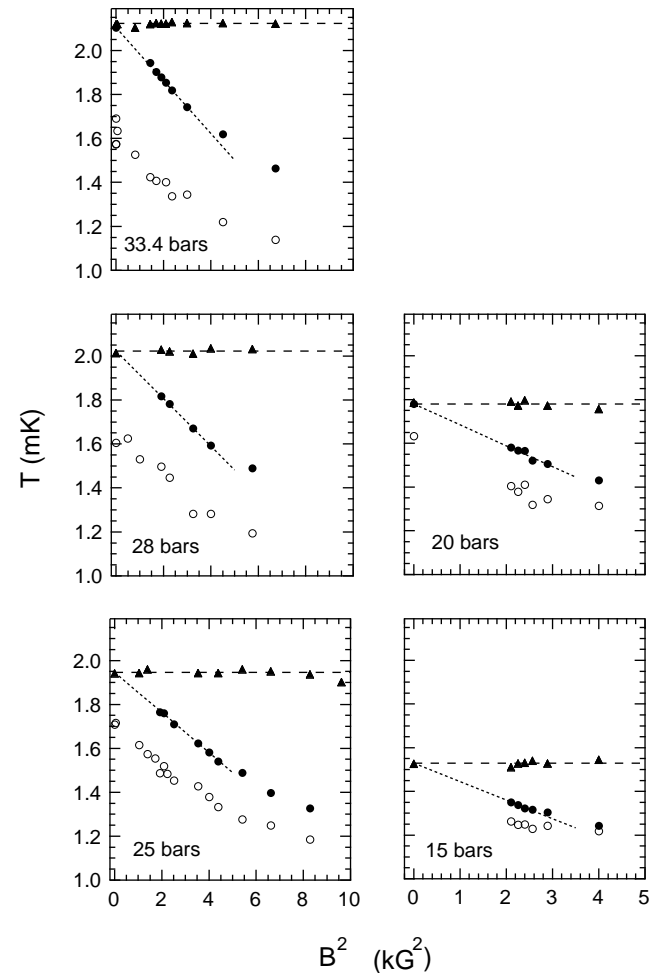


FIG. 3. Phase diagrams of the superfluid phases in aerogel at various pressures in a magnetic field. The triangles are the superfluid transition temperature, T_{ca} , determined from transverse acoustics. The supercooled aerogel AB-transitions, T_{ABa} , are shown on cooling (empty circles) and in equilibrium on warming (filled circles). The data are plotted as function of B^2 to illustrate the quadratic suppression of the AB-transition at low field. The dashed lines show the average value of T_{ca} and the dotted lines are an extrapolation of T_{ABa} to zero field. Note that the field axis is different for the left and right panels.

Fig.4 shows these various traces upon warming to a temperature in the vicinity of T_{ca} (lower panel and traces labeled 1 to 4, vertically offset for clarity), and then rapidly cooled. The thermal disequilibrium during sud-

den cooling is sufficient to make the cooling traces appear to move up in this figure. The lowest trace shows the complete acoustic record with T_{ca} indicated by a change of slope and marked by a solid vertical line.

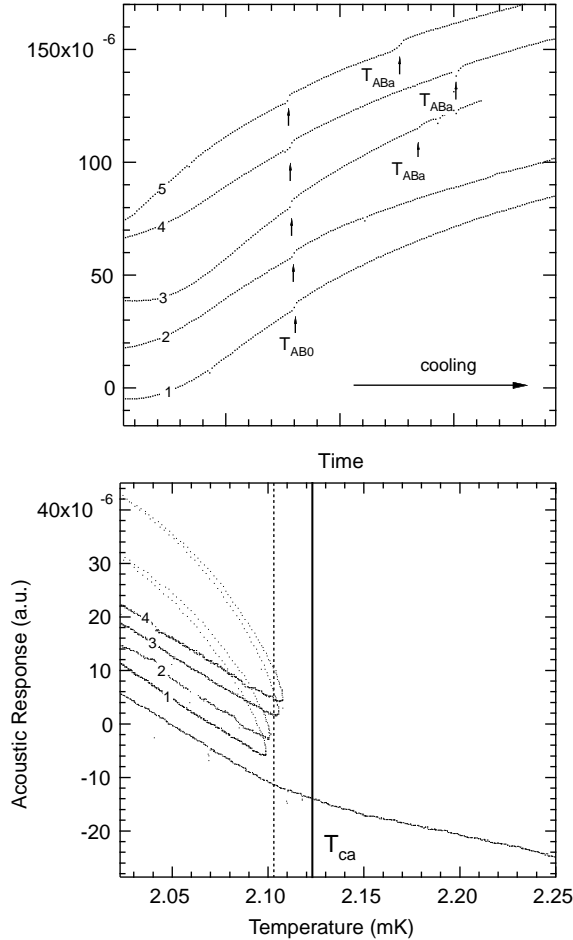


FIG. 4. Lower panel: transverse acoustic response at 33.4 bars and zero applied field during slow warming in the vicinity of T_{ca} and subsequent rapid cooling. The traces labeled 1 to 4 correspond to several maximum temperatures reached prior to rapid cooling. The corresponding cooling traces are shown in the upper panel as a function of time and the bulk and aerogel AB-transitions are denoted by arrows. For traces 1 and 2 the aerogel AB transition was not crossed on warming and for traces 3 and 4 it was. The trace labeled 5 shows the aerogel AB-transition but for a cooling experiment originating from the normal state. In the lower panel, the vertical solid line is T_{ca} as determined from the change in slope of the acoustic response on warming, and the dotted line is a lower bound on the temperature for the aerogel AB-phase boundary, $\sim 20 \mu\text{K}$ below T_{ca} .

In the upper panel, we show the same acoustic traces for rapid cooling (1 to 4) as a function of time while the trace labeled 5 is for a cooling experiment originating from the normal state. We do not observe the aerogel AB-transition upon cooling in the trace 1 and 2 (and also for any partial warmup to temperatures below those

shown here), while in the traces 3 and 4 the aerogel AB-transition is observed on cooling. This shows that the equilibrium aerogel AB-transition lies at a temperature somewhere between the traces 2 and 3, which is indicated in the lower panel of Fig.4 by a dotted line. This is close to T_{ca} ($\lesssim 20 \mu\text{K}$) and is approximately the width of T_{ca} itself ($\sim 30 \mu\text{K}$), sufficiently close that we cannot say that the normal state of the ^3He fluid in aerogel had not been reached somewhere in the sample. Consequently, we have inferred that the region of A-phase in aerogel in zero applied field is extremely narrow, $\lesssim 20 \mu\text{K}$ at a pressure of 33.4 bars. We have also verified at a pressure of 20 bars that the AB-phase boundary in zero applied field is indistinguishable from T_{ca} using the same slow warming and quench-cooling method.

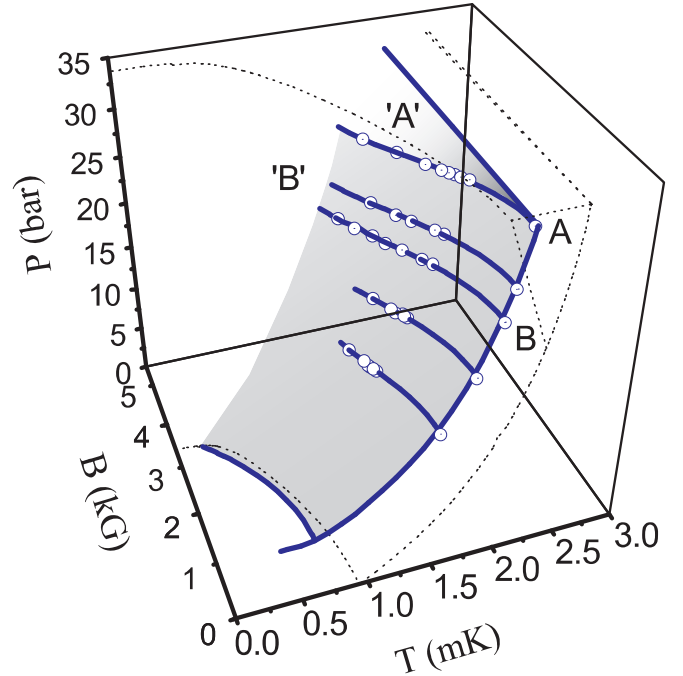


FIG. 5. Three-dimensional phase diagram (P, T, B) of the A and B superfluid phases of ^3He in 98% aerogel. The aerogel phases are labeled 'A' and 'B' and are delineated by solid lines while for the pure phases they are labeled A and B and shown with dotted lines. The shaded area shows the volume spanned by the equilibrium A-phase in aerogel. The open circles are data from the present work, and the lines connecting them are fits to the data. At pressures below 10 bars, T_{ca} , was taken from Matsumoto *et al.*³⁴, together with the field dependence of the AB-transition observed by the Lancaster group at 4.8 bars²⁶.

From the data of Fig.3 we construct a three-dimensional phase diagram for pressure, temperature and magnetic field for the superfluid phases of pure ^3He in 98% aerogel, Fig.5. The relative stability of the superfluid phases of the pure and dirty superfluids can be directly visualized and compared. The data of the equilibrium AB-transition from Fig.3 are shown as empty cir-

cles, and the thick solid lines are a smoothed fit of T_{ABA} and T_{ca} . Below 10 bars, the data from Matsumoto *et al.*³⁴ were used to describe T_{ca} . They found a critical pressure of ~ 6 bars in the zero-temperature limit. The thick solid curve at a pressure of 4.8 bars was taken from the field dependence of the aerogel AB-transition measured by the Lancaster group with a vibrating viscometer²⁶, but with its superfluid transition adjusted to match that of Matsumoto *et al.*³⁴. Above 10 bars our data for T_{ca} in zero field are similar from that of Matsumoto *et al.*³⁴ and the data points are not shown for reasons of clarity. The aerogel phases are denoted by ‘A’ and ‘B’ while the pure phases are denoted by A and B. The shaded volume emphasizes the aerogel A-phase opening up with applied magnetic field, and the dotted lines are the pure phase diagram shown here for comparison³⁶. The field dependence of the aerogel superfluid transitions T_{ca} plotted as a solid line at 33.4 bars will be discussed later.

The three-dimensional plot of the (P,T,B) phase diagram of ^3He in 98% aerogel shows the effects of impurity scattering on the equilibrium A-phase. The equilibrium region of A-phase is destabilized by impurity scattering in zero field; however, we believe that there is a very thin sliver of equilibrium A-phase that gives rise to supercooling of the A-phase observed in zero applied field²⁷ at pressures above 15 bars. Barker *et al.*¹⁵ observed a metastable aerogel AB-transition on cooling using an NMR technique at 284 G and with ^4He preplating. At 32 bars, an equilibrium region of A-phase of $70 \mu\text{K}$ was inferred from the data. This is somewhat larger than our results at the same field. The magnetization discontinuity at the AB-transition known to occur in the bulk system was not observed in aerogel, making it difficult to locate the equilibrium AB-transition. Furthermore, given the scatter of the data¹⁵ and the thermometry resolution $\sim 20 \mu\text{K}$, it seems plausible that the A-phase region might have been smaller than $70 \mu\text{K}$ and consistent with our findings here.

B. Magnetic suppression of the AB-transition and the Homogeneous Scattering Model

The Ginzburg-Landau (GL) theory for superfluid ^3He describes the free energy near the transition temperature expanded in powers of the order parameter. With this approach the relative stability of various possible p -wave states can be explored in terms of the expansion coefficients of the theory³⁷. An extension to the dirty superfluid has been developed¹¹ using a model that describes elastic quasiparticle scattering. There are five possible fourth order combinations of the order parameter that are invariant under all the symmetries of the p -wave superfluid. These fourth-order terms are characterized by the coefficients, $(\beta_1, \beta_2, \beta_3, \beta_4, \beta_5)$, which in the GL-theory are determined by thermodynamic quantities such as heat capacity, the magnetization, the phase diagram and the NMR frequency shift. In principle one

could uniquely determine the β_i ’s (thus the free energy functional) if five independent thermodynamic measurements were performed; the fact that in bulk superfluid ^3He there are only four such measurements is unfortunate. Nonetheless, combinations of the β_i ’s can be extracted from experiment and are very helpful in the understanding the magnetic suppression of the B-phase of ^3He in aerogel.

In the pure superfluid the GL-theory can be used to describe the suppression of the AB-transition by magnetic field only for pressures less than 21 bars, the pressure of the polycritical point. For superfluid ^3He in aerogel, the data from Fig.3 suggest that this theory can be applied at all pressures with

$$1 - \frac{T_{ABA}}{T_{ca}} = g_a(\beta) \left(\frac{B}{B_0} \right)^2 + \mathcal{O} \left(\frac{B}{B_0} \right)^4, \quad (2)$$

where $g_a(\beta)$ is a strong-coupling parameter defined in a manner similar to that of the pure superfluid and B_0 is defined as,

$$B_0 = \sqrt{\frac{8\pi^2}{7\zeta(3)}} \frac{k_B T_{ca}}{\gamma\hbar} (1 + F_0^a), \quad (3)$$

with γ the gyromagnetic ratio of ^3He and F_0^a is a Fermi liquid parameter. In the Homogeneous Scattering Model (HSM) which we describe below, B_0 is modified by impurity scattering according to^{24,20}

$$B_0^{HSM}/B_0 = \sqrt{\frac{7\zeta(3)[1 - x \sum_{n=1}^{\infty} (n - 1/2 + x)^{-2}]}{\sum_{n=1}^{\infty} (n - 1/2 + x)^{-3}}} \quad (4)$$

where $x \equiv \hbar v_f / 4\pi k_B T_{cal, tr}$ and l_{tr} is the transport mean free path. This correction is about 2.5% at 25 bars with a 200 nm mean free path. We use the weak coupling approximation in Eq.3 which has been shown to be appropriate for bulk ^3He ³⁸. Assuming that the aerogel AB-transition occurs between the axial and the isotropic states, as in the pure superfluid, the coefficient $g_a(\beta)$ is written as,

$$g_a(\beta) = \frac{\beta_{245}}{2(-3\beta_{13} + 2\beta_{345})} \times \quad (5)$$

$$\left(1 + \sqrt{\frac{(3\beta_{12} + \beta_{345})(2\beta_{13} - \beta_{345})}{\beta_{245}\beta_{345}}} \right) \quad (6)$$

where we have used the Mermin-Stare convention, $\beta_{ijk} \equiv \beta_i + \beta_j + \beta_k$. In the weak-coupling limit, $-\beta_5^{wc} = \beta_4^{wc} = \beta_3^{wc} = \beta_2^{wc} = -2\beta_1^{wc} = 2\beta_0$ with $\beta_0 = 7\zeta(3)N(0)/8(\pi k_B T_{c0})^2$, and $N(0)$ is the zero-temperature density of states. In the weak-coupling limit, $g_a(\beta^{wc}) = 1$.

The coefficient $g_a(\beta)$ can be taken directly from the low-field slope, m , of the data in Fig.3, $m = -g_a(\beta)T_{ca}/B_0^2$. In Fig.3, the dotted lines show the quadratic suppression of T_{ABA} for the smallest field at

which the transition was observed, and the extrapolation to zero field was verified using the quench-cooling method we have described above, see Fig.4. The pressure dependence of $g_a(\beta)$ obtained from the data between 15 and 33.4 bars is shown in Fig.6 (filled circles), together with the measured values from the bulk, $g_0(\beta)$, taken from Hahn *et al.*³⁶ (open circles). For the aerogel data $g_a(\beta)$, B_0 as defined as in the pure case was used; using the HSM correction B_0^{HSM} increases slightly the value of $g_a(\beta)$, however, its effect for a mean free path of ~ 200 nm remains within the experimental error bar. For this reason and for clarity, we have used B_0 which does not depend on the transport mean free path. We have also deduced the value of $g_a(\beta)$ at 4.8 bars from the magnetic suppression of the aerogel AB-transition measured by the Lancaster group²⁶ and denoted in Fig.6 as a star. The solid line is a guide-to-the-eye and the dotted, dashed, and dot-dashed lines are calculations using the homogeneous scattering model (HSM) which we discuss below. The pressure dependence of $g_a(\beta)$ is markedly different from the pure superfluid, $g_0(\beta)$, which diverges at the PCP near 21 bars. The almost linear dependence on pressure observed in the aerogel superfluid, even at high pressure, is a substantial modification of the phase diagram induced by impurity scattering.

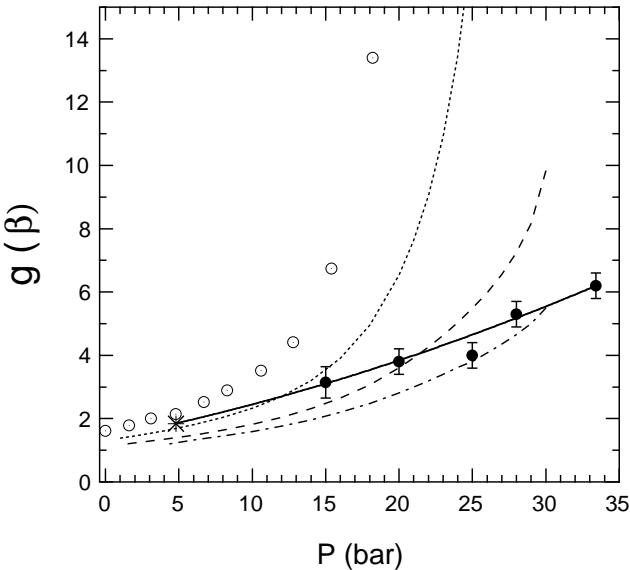


FIG. 6. Pressure dependence of the strong-coupling coefficient $g(\beta)$. The aerogel data from the present work (solid circles) are compared to the bulk (empty circles)³⁶. The data at 4.8 bars denoted by a star are from Brussard *et al.*²⁶. The solid line is a guide-to-the-eye. The dotted line is the HSM with $l_{tr} = 270$ nm and for which the pure ^3He strong-coupling corrections are used. The same model was used with strong-coupling corrections rescaled from pure ^3He by the factor T_{ca}/T_{c0} and two values of transport mean free path were chosen, $l_{tr} = 270$ nm (dashed) and 200 nm (dot-dashed).

The simplest model of impurity scattering is the Homogeneous Scattering Model (HSM)¹¹. In this model, the scattering probability is independent of position and the medium is completely isotropic. This model has the advantage that the Ginzburg-Landau theory is only slightly modified from that of pure ^3He . The superfluid transition in aerogel, T_{ca} , is given by solving Eq.1 in the form,

$$\ln(T_{ca}/T_{c0}) + \sum_{n=1}^{\infty} \left(\frac{1}{n - \frac{1}{2}} - \frac{1}{n - \frac{1}{2} + x} \right) = 0 \quad (7)$$

where $x \equiv \hbar v_f / 4\pi k_B T_{cal, tr}$ and l_{tr} is the transport mean free path. The β_i 's have been calculated for the HSM and are given by¹¹,

$$\begin{pmatrix} \beta_1/\beta_0 \\ \beta_2/\beta_0 \\ \beta_3/\beta_0 \\ \beta_4/\beta_0 \\ \beta_5/\beta_0 \end{pmatrix} = a_1 \begin{pmatrix} -1 \\ 2 \\ 2 \\ 2 \\ -2 \end{pmatrix} + a_2 \begin{pmatrix} 0 \\ 1 \\ 0 \\ 1 \\ -1 \end{pmatrix} + \begin{pmatrix} \delta\beta_1^{sc}/\beta_0 \\ \delta\beta_2^{sc}/\beta_0 \\ \delta\beta_3^{sc}/\beta_0 \\ \delta\beta_4^{sc}/\beta_0 \\ \delta\beta_5^{sc}/\beta_0 \end{pmatrix} \quad (8)$$

where the coefficients, a_1 and a_2 , are given by,

$$a_1 = \left(\frac{T_{c0}}{T_{ca}} \right)^2 \frac{\sum_{n=1}^{\infty} (n - \frac{1}{2} + x)^{-3}}{7\zeta(3)}, \quad (9)$$

$$a_2 = \frac{5}{6} \frac{\hbar v_f}{\pi k_B T_{cal, tr}} \left(\frac{T_{c0}}{T_{ca}} \right)^2 \left(\sin^2 \delta_0 - \frac{1}{2} \right) \frac{\sum_{n=1}^{\infty} (n - \frac{1}{2} + x)^{-4}}{7\zeta(3)} \quad (10)$$

and the $\delta\beta_i^{sc}$'s are the strong-coupling corrections to the free energies. Note that in the bulk limit ($l_{tr} \rightarrow \infty$), $a_1 \rightarrow 1$ and $a_2 \rightarrow 0$. We choose a random scattering phase shift δ_0 such that $\sin^2 \delta_0 = 1/2$ and $a_2 = 0$. Calculations performed with a scattering phase shift in the unitary limit ($\sin^2 \delta_0 = 1$) or Born limit ($\sin^2 \delta_0 = 0$) have only a small effect on the magnitude of $g_a(\beta)$ and do not alter our conclusions. The strong-coupling corrections, essential to calculate accurately $g_a(\beta)$, are taken from pure ^3He ³⁸; namely, β_{345} is derived from measurements of the B-phase NMR g-shifts and longitudinal resonance frequency³⁸, β_{12} from the normal to B-phase heat capacity jump³⁹, and β_{245} and β_5 are from measurements of the $A_1 - A_2$ splitting⁴⁰ and magnetic suppression of the bulk AB-transition, $g_0(\beta)$ ³⁶. The only unknown parameter in the HSM is the transport mean path, l_{tr} , for which high-frequency acoustic measurements on our sample have determined that it should be in the range 200-300 nm^{31,33}. In all of the calculations, T_{ca} was solved using Eq. 7 and was used consistently throughout our calculations of the β_i 's.

In Fig.6, the dotted line shows the calculations of $g_a(\beta)$ which assumes that the strong-coupling corrections are the same as in the pure superfluid and with a transport mean free path of 270 nm, fixed by our experimental value of T_{ca} at $P \sim 25$ bars. The effect of scattering is to increase the polycritical pressure, where $g_a(\beta)$ diverges, thus increasing the stability of the dirty B-phase.

This model does not describe our experimental data for any reasonable value of the transport mean free path. However, we expect that the strong-coupling corrections should be rescaled to first-order as $\delta\beta_i^{sc} \sim (T_c/T_F)\beta_0$, hence being reduced in the dirty system accordingly to $(\delta\beta_i^{sc})_a \simeq (\delta\beta_i^{sc})_{bulk} \times \frac{T_{ca}}{T_{c0}}$ where $(\delta\beta_i^{sc})_a$ and $(\delta\beta_i^{sc})_{bulk}$ are the strong-coupling corrections in the dirty and the pure superfluids. In Fig.6 the calculations of $g_a(\beta)$ were also performed with the HSM using the rescaled strong-coupling coefficients. They are shown with two choices of transport mean free path of 270 nm (dashed line) and 200 nm (dot-dashed line) which are within the range allowed by our earlier measurements³¹. Considering the limitations of the HSM, the agreement between the data and calculated $g_a(\beta)$, for either value of the mean free path, is reasonably good. More importantly, it shows unambiguously that the strong-coupling corrections are reduced by impurity scattering and that the PCP is increased in a 98% porous aerogel above the melting pressure, beyond experimental reach. At the PCP, the heat capacity jump in the A-phase equals that of the B-phase, equivalent to the condition, $3\beta_{13} = 2\beta_{345}$ in Eq. 6. The HSM with rescaled strong-coupling corrections, predicts a PCP of ~ 35 bars for a mean free path of 270 nm and a PCP of ~ 40 bars for a mean free path of 200 nm. The almost linear dependence on pressure of $g_a(\beta)$ that we observe suggests that the true PCP may even be higher than estimated from the HSM. Experiments with higher porosity aerogels, having a correspondingly larger mean free path, may be able to clarify this situation. It might also be necessary to take into account modification of the strong-coupling corrections beyond a simple rescaling as we have done, *e.g.* the effect of impurities on spin-fluctuation feedback⁴¹.

The agreement of our data with the the HSM calculations using a rescaling of the strong coupling corrections to the β_i 's provides qualitative evidence that the orbital symmetry of the order parameter in the aerogel system is similar to that of the pure superfluid. The expression, Eq. 4, for suppression of the AB-transition is specific to the transition between axial and isotropic states and so the agreement between the model and our measurements of the transition is consistent with, but not a proof of, their identification with A and B phases in the dirty superfluid.

Finally, it is worth noting that in the pure superfluid $g_0(\beta)$ does not recover its weak-coupling value (1) at zero pressure, but rather takes the value 1.61³⁶. This rather large deviation from weak-coupling theory at zero pressure, $\sim 40\%$, is unexpected since all other thermodynamic measurements indicate much smaller deviations from weak coupling at low pressure. At zero pressure, the B-phase heat capacity jump³⁹ and $A_1 - A_2$ linear field splitting⁴⁰ are within 3% of their weak-coupling values. This finite contribution to $g_0(\beta)$ at zero pressure has been interpreted as evidence that ^3He is not a weak-coupling superfluid at zero pressure³⁶. As we have shown above, the strong-coupling corrections are reduced by scattering

(scaling with T_{ca}) and should therefore be dramatically reduced at low pressure where T_{ca} is most strongly suppressed. We therefore expect $g_a(\beta)$ to recover its weak-coupling limit in aerogel at low pressure, if indeed the deviation of $g_0(\beta)$ from weak coupling in pure ^3He at low pressure is due to strong-coupling corrections. Our data in aerogel do not allow us to extrapolate to zero pressure and so an accurate measurement of $g_a(\beta)$ at low pressures would be desirable since it might shed light on this problem.

C. Field dependence of T_{ca}

The field dependence of T_{ca} at 33.4 bars is shown in Fig.7 for fields ranging from 0 to 5 kG. The transition is clearly field independent and from this we can infer that the superfluid transition is from a normal fluid to an ESP superfluid. These data contradict earlier NMR work where a B^2 field dependence was reported for the superfluid transition in aerogel¹⁰. Upon reanalysis of these same earlier results including some additional experiments, by Haard³⁸, it was found that the NMR data are consistent with the acoustic experiments presented here to within experimental error.

In pure superfluid ^3He , owing to particle-hole asymmetry, a magnetic field produces a linear splitting of the normal to A-phase transition⁴⁰. The field dependence of the splitting between the A_1 and A_2 phase lines is 6 $\mu\text{K}/\text{kG}$ near melting pressure and is shown in Fig.7 as dotted lines shifted to the average value of T_{ca} .

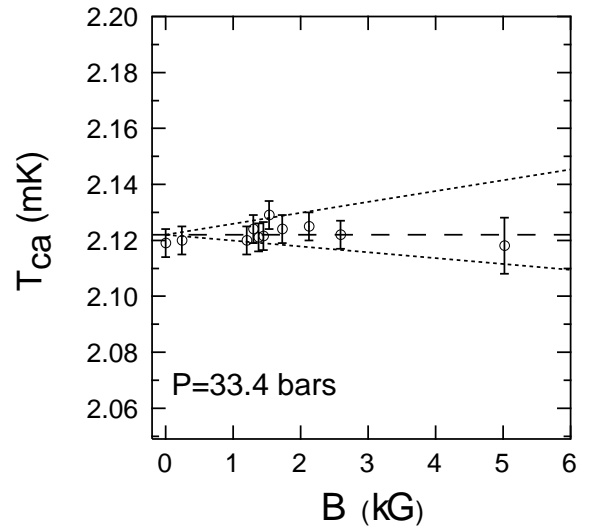


FIG. 7. Field dependence the aerogel superfluid transition T_{ca} at 33.4 bars. The dashed line shows the average value of T_{ca} . The slopes of the two dotted lines are the same as for the $A_1 - A_2$ splitting measured for pure ^3He near melting pressure⁴⁰.

In contrast, for the aerogel superfluid we do not observe any deviation of T_{ca} from its zero-field value, nor

do we observe significant broadening of the transition region in the acoustic trace even at our highest field of 8 kG (not shown in Fig.7. This splitting may be hard to resolve owing to the rather broad superfluid transition in aerogel, $\sim 30\mu K$. The expected linear $A_1 - A_2$ splitting in the dirty superfluid can be estimated from calculations based on Ginzburg-Landau theory and the HSM (see above). The bulk $A_1 - A_2$ splitting can be expressed by the quantity U_0 defined as,³⁶

$$U_0 \equiv -\frac{(dT/dB)_{A1}}{(dT/dB)_{A2}} = -\frac{\beta_5}{\beta_{245}}. \quad (11)$$

which ranges for pure ^3He from 0.97 at zero pressure to 1.81 at melting pressure. In the HSM, the U parameter can be calculated from β_5 and β_{245} and in aerogel takes the value at melting pressure of $U_a \simeq 0.8U_0$ with a mean free path of 270 nm. For this estimate, we have used the rescaled bulk strong-coupling corrections as discussed above. Measurements of T_{ca} in high fields sufficient to resolve this splitting are desirable in order to establish a better understanding of the thermodynamics of the dirty superfluid.

D. Supercooling of the aerogel AB-transition in zero applied field

We have shown that the polycritical point vanishes for superfluid ^3He in 98% aerogel. Consequently, in zero field we expect that superfluidity occurs by a second order transition from the normal state directly to the B-phase without supercooling. Our observation of supercooling giving a large region of metastable A-phase *with no applied field* is quite unexpected. Supercooling was first noted by Barker *et al.*¹⁵ for the aerogel AB-transition at 284 G with ^4He preplating. This was also found for zero applied field and was studied as a function of magnetic field by Gervais *et al.*^{27,35}. Our smallest field in this case was estimated to be less than 10 G. There are a number of possible interpretations and so a review of the expected behavior in the limit of low magnetic field is appropriate.

Taking pure superfluid ^3He as a guide, the first transition encountered on cooling in a small but non-zero magnetic field is from the normal state to the A_1 -phase and then, in the absence of supercooling, to the B-phase. If there were to be supercooling it is likely that the A_2 transition would be encountered before reaching the B-phase. This follows since the A_1 transition increases linearly with field whereas the B-phase is suppressed quadratically. Consequently, the supercooling of the aerogel AB-transition at 284 G observed by Barker *et al.*¹⁵ can be explained in a trivial way: a small region of A_1 -phase in equilibrium, $\lesssim 1\mu K$, is first encountered on cooling, leading to a metastable A-phase that supercools until the B-phase nucleates. However, the mechanism for producing relative stability of one phase over another, or the nucleation of the most stable phase, has not been explored in such a small interval of temperature near T_c .

Can the same argument for supercooling in 284 G hold at very low field as well? If the total field for the case of zero applied field were less than 10 G then the window of stability of the A_1 -phase would be only $\lesssim 0.03\mu K$. We find supercooling under these circumstance to be even more remarkable since there is no evidence of similar supercooling for the pure superfluid at pressures below the polycritical point. If the phenomenon of supercooling in low field were to be unique to the dirty superfluid then it would require a correspondingly unique nucleation scenario specific to the aerogel AB-transition, which, in addition, must also account for our observation that the extent of supercooling is field independent²⁷. Furthermore, it seems not to make sense to rely on details for phase stability in such a narrow window of temperature when the superfluid transition T_{ca} is inhomogeneously broadened over an interval three orders of magnitude larger. A second possibility, and one that we believe to be more likely, is that there must be a thin, but unobserved, sliver of A-phase near T_{ca} which gives rise to the metastability that is observed. This sliver is at most $\lesssim 20\mu K$ wide, but might be stabilized by inhomogeneity in the aerogel structure in a manner that is not yet understood. In Fig.8, the metastable phase diagram from Gervais *et al.*²⁷ is shown with no applied magnetic field ranging in pressure from 15 to 33.4 bars. The region of metastability is strikingly similar to that observed by Barker *et al.*¹⁵ in a field of 284 G, with ^4He preplating, and for a much larger aerogel sample. The critical radius R_c for B-phase nucleation may play an important role, since a large critical radius in the aerogel might give rise to the observed metastability. An estimate³⁵ near melting pressures from the susceptibility difference and field dependence of T_{ABa}^{ABa} shows that it is slightly larger in aerogel, $R_c^{aero} \sim 5R_c^{bulk}$, at the same value of T/T_{AB} . In pure ^3He the critical radius has not been measured below melting pressure. Future work in a magnetically shielded environment and with different aerogel densities, together with characterization of R_c as a function of pressure, could bring some understanding to this puzzle.

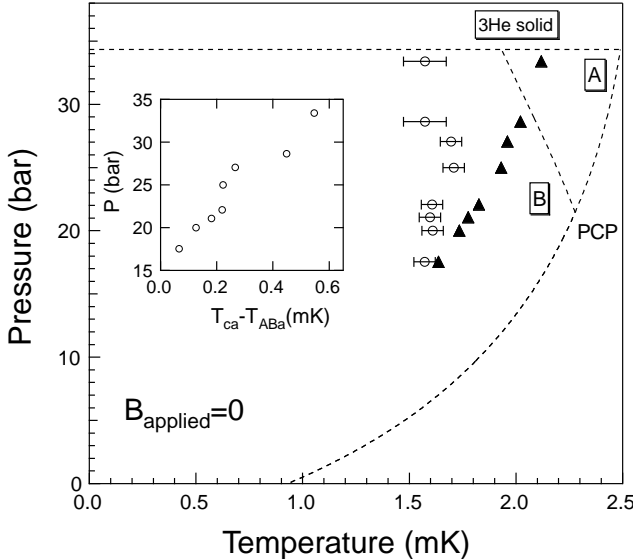


FIG. 8. Phase diagram for metastable ^3He A-phase in 98% porous aerogel in zero applied magnetic field. The triangles are the aerogel superfluid transition and the open circles the aerogel A-B transition on cooling. The inset shows the magnitude of supercooling of the aerogel A-B transition as a function of pressure. The dotted lines are the pure ^3He superfluid phase with A, B and solid phases indicated.

For all experiments to date it has been unavoidable that pure and dirty superfluids be juxtaposed. In future work it may be possible to explore the connection between these two unconventional superfluids and such experiments can benefit from detailed knowledge of the phase diagram. In this spirit we have recently investigated the nucleation of the AB-transition³⁵ showing that proximity coupling between the pure and dirty superfluids is too weak to act as a source of nucleation.

IV. CONCLUSION

We have described the phase diagram of superfluid ^3He in 98% aerogel. In this phase diagram we find two equilibrium states which we call A and B, by analogy with pure ^3He . The B-phase is favored in zero field and is destabilized by a magnetic field yielding the A-phase. The superfluid transition from the normal state, *i.e.* normal to A-phase transition, is insensitive to magnetic field. On this basis alone we can be confident of the nature of the spin part of the order parameter associated with each of these phases: the A-phase is an equal spin pairing state and the B-phase is a non-equal spin pairing state. The field dependence of the AB-transition can be understood from calculations using the HSM model combined with a simple rescaling of strong-coupling corrections to the quasiparticle interactions, assuming that the A and B dirty phases are in fact the axial and isotropic p -wave states. The theory and experiment both concur that sufficient impurity scattering, as is the case for 98% aerogel,

causes the polycritical point to vanish. It is intriguing that no hint of the expected but small $A_1 - A_2$ splitting was observed even at fields of ~ 8 kG; however, higher field experiments will be better able to address this question.

The extensive supercooling of the AB-transition, especially with no applied field, remains a puzzle. It cannot be simply explained in terms of the phase diagram that we present, nor in terms of current nucleation scenarios. This raises further questions concerning the nature of the superfluid state in aerogel and whether it might be inherently inhomogeneous.

In summary, the measurements of the equilibrium phase diagram of ^3He with impurity scattering improves our understanding of pure and dirty superfluids and sets the stage for a better understanding of its non-equilibrium behavior, metastability and nucleation.

ACKNOWLEDGMENTS

We acknowledge helpful discussions with J.A. Sauls. Work supported by the NSF under grant no. DMR-0072350. One of the author (G.G) acknowledges receipt of support from FCAR (Québec).

- ¹ X.-l. Wu, W.I. Goldburg, M.X. Liu and J.Z. Xue, Phys. Rev. Lett. **69**, 470 (1992).
- ² M.H. W. Chan, K.I. Blum, S.Q. Murphy, G.K.S Wong, and J.D. Reppy, Phys. Rev. Lett. **61**, 1950 (1988).
- ³ S.B. Kim, J. Ma, and M.H.W. Chan, Phys. Rev. Lett. **71**, 2268 (1993).
- ⁴ J.V. Porto and J.M. Parpia, Phys. Rev. Lett. **74**, 4667 (1995).
- ⁵ D.T. Sprague *et al.*, Phys. Rev. Lett. **75**, 661 (1995).
- ⁶ D.D. Osheroff, R.C. Richardson, and D.M. Lee, Phys. Rev. Lett. **28**, 885 (1972).
- ⁷ Y. Maeno, T.M. Rice, and M. Sigrist, Physics Today, January 2001 p.42.
- ⁸ D. Aoki *et al.*, Nature, **413**, 613, (2001).
- ⁹ S. Lefebvre *et al.*, Phys. Rev. Lett. **85**, 5420 (2000).
- ¹⁰ D.T. Sprague *et al.*, Phys. Rev. Lett. **77**, 4568 (1996).
- ¹¹ E.V. Thuneberg, S.K. Yip, M. Fogelstrom, and J.A. Sauls, Phys. Rev. Lett. **80**, 2861 (1998).
- ¹² H. Alles, J.J. Kaplinsky, P.S. Wootton, J.D. Reppy, J.H. Naish, and J.R. Hook, Phys. Rev. Lett. **83**, 1367 (1999).
- ¹³ A. Golov, D.A. Geller, J.M. Parpia, and N. Mulders, Phys. Rev. Lett. **82**, 3492 (1999).
- ¹⁴ A. Matsubara *et al.*, Physica B **284**, 301 (2000).
- ¹⁵ B.I. Barker, Y. Lee, L. Polukhina, D.D. Osheroff, L.W. Hrubesh and J.F. Poco, Phys. Rev. Lett. **85**, 2148 (2000); B.I. Barker, Ph.D. thesis, Stanford University, 2000, (unpublished).

¹⁶ Yu. M. Bunkov, A.S. Chen, D.J. Cousins, and H. Godfrin, Phys. Rev. Lett. **85**, 3456 (2000).

¹⁷ G. Lawes, S.C.J. Kingsley, N. Mulders and J.M. Parpia, Phys. Rev. Lett. **84**, 4148 (2000).

¹⁸ G.E. Volovik, Pis'ma Zh. Eksp. Teor. Fiz. **63**, 281 (1996) [JETP Lett. **63**, 301 (1996)].

¹⁹ G. Baramidze, G. Kharadze, and G. Vachnadze, Pis'ma Zh. Eksp. Teor. Fiz. **63**, 95 (1996), [JETP Lett. **63**, 107 (1996).]

²⁰ E.V. Thuneberg, in *Quasiclassical Methods in Superconductivity and Superfluidity*, Verditz 96, ed. D. Rainer and J.A. Sauls (1998) p.53 (also cond-mat/982044).

²¹ R. Hänninen, T. Setälä and E.V. Thuneberg, Physica B **255**, 11 (1998).

²² D. Einzel and J.M. Parpia, Phys. Rev. Lett. **81**, 3896 (1998).

²³ S. Higashitani, J. Low Temp. Phys. **114**, 161 (1999).

²⁴ P. Sharma and J.A. Sauls, J. Low Temp. Phys. **125**, 115 (2001).

²⁵ V.P. Mineev and P.L. Krotkov, Phys. Rev. **B65**, 024501 (2002).

²⁶ P. Brussaard, S.N. Fisher, A.M. Guénault, A.J. Hale, N. Mulders and G.R. Pickett, Phys. Rev. Lett. **86**, 4580 (2001).

²⁷ G. Gervais, T. M. Haard, R. Nomura, N. Mulders and W. P. Halperin, Phys. Rev. Lett. **87**, 035701 (2001).

²⁸ W.R. Abel, A.C. Anderson and J.C. Wheatley, Phys. Rev. Lett. **17**, 74 (1966).

²⁹ W.P. Halperin and E. Varoquaux, Helium Three, eds. W.P. Halperin and L.P. Pitaevski (Elsevier, Amsterdam), 255 (1990).

³⁰ Y. Lee, T. M. Haard, W.P. Halperin and J.A. Sauls, Nature **400**, 431 (1999).

³¹ R. Nomura., G. Gervais, T.M. haard, Y. Lee, N. Mulders and W.P. Halperin , Phys. Rev. Lett. **85**, 4325 (2000).

³² P.R. Roach and J.B. Ketterson, J. Low Temp. Phys. **25**, 637 (1976).

³³ G. Gervais, R. Nomura, T.M. Haard, Y. Lee, N. Mulders and W.P. Halperin, J. Low Temp. Phys. **122**, 1 (2001).

³⁴ K. Matsumoto, J.V. Porto, L. Pollack, E.N. Smith, T.L. Ho, and J.M. Parpia, Phys. Rev. Lett. **79**, 253 (1997).

³⁵ G. Gervais, K. Yawata, N. Mulders and W.P. Halperin, Phys. Rev. Lett. **88**, 045505 (2002).

³⁶ Y.H. Tang, I. Hahn, H.M. Bozler, and C.M. Gould, Phys. Rev. Lett. **67**, 1775 (1991); I. Hahn, Ph.D. thesis, University of Southern California, 1993, (unpublished).

³⁷ N.D. Mermin and C. Stare, Phys. Rev. Lett. **30**, 1135 1973.

³⁸ T.M. Haard and W.P. Halperin, to be published; T.M. Haard, Ph.D. thesis, Northwestern University, 2001 (unpublished).

³⁹ D.S. Greywall, Phys. Rev. **B33**, 7520 (1986).

⁴⁰ U.E. Isrealsson, B.C. Crooker, H.M. Bozler, and C.M. Gould, Phys. Rev. Lett. **53**, 1943 (1984).

⁴¹ G. Baramidze and G. Kharadze, cond-mat/0111161 (unpublished).